Direct displacement-based seismic design of flexible-base structures subjected to pulse-like ground motions

Yang Lu[1*], Iman Hajirasouliha[2], Alec M. Marshall[3]

[1] *College of Architecture and Environment, Sichuan University, PRC*

[2]*Department of Civil & Structural Engineering, The University of Sheffield, UK*

[3]*Department of Civil Engineering, University of Nottingham, UK*

[*]*Corresponding Author: E-mail: yang.lu@scu.edu.cn*

ABSTRACT

In this paper, a practical displacement-based framework is presented for seismic design of flexible-base structures in near-fault regions. Particular attention is given to pulse-like motions that may cause significant damage to building structures. The proposed design methodology utilises displacement response spectra constructed using a new procedure, which takes into account the effect of pulse period. An equivalent fixed-base single-degree-of-freedom oscillator is adopted to capture the salient features of an actual soil-structure interaction (SSI) system in order to facilitate the design process. Two step-by-step direct-displacement based design (DDBD) procedures based on compatible inelastic spectra and equivalent linearisation are introduced. The effectiveness of the stated design procedures is examined using results of nonlinear response history analysis of two example SSI systems subjected to a set of sixteen spectrum-compatible near-fault pulse-like ground motions. The results of this study suggest that the procedure based on inelastic design spectra, in general, provides a better design solution than using an elastic linearisation method, especially when structures are designed with a higher ductility demand.

Key words: Direct-displacement based design; soil-structure interaction; velocity pulse; near-fault ground motion; inelastic spectra

1. INTRODUCTION

Structures located near causative faults are prone to extensive damage in strong earthquakes, especially when ground motions contain distinguishable pulses whose periods are close to those of the buildings. A well-known phenomenon that may lead to velocity pulses is the "forward directivity" effect due to the propagation of fault rupture at a velocity close to the local site shear wave velocity. Compared to far-field ground motions that build up energy more gradually within structures, these pulse-like motions (e.g. the fault-normal components of ground motions) can expose structures to high input energy at the beginning of shaking [1]. Note that in addition to the velocity pulses, high-frequency components of near-fault ground motions may also cause adverse effects on short stiff structures [2,3].

The effects of pulse-like motions on building response have been studied by a number of researchers. Alavi and Krawinkler [4] demonstrated that the storey shear force distribution within a 20-storey moment-resisting steel frame varied significantly with the pulse period T_P (i.e. duration of the distinct ground velocity pulse). In their study, the pulse period was defined based on three mathematical square-wave acceleration pulses that represented a set of 15 near-fault earthquake records. Akkar *et al*. [5] showed that the maximum inter-storey drift ratio of steel frame systems exhibited noticeably higher values when the fundamental period of the building T_s approached the pulse period T_P, which was measured directly from the ground velocity time series. The results of the stated studies were confirmed by Kalkan and Kunnath [6] by utilising sinusoidal wave shapes to simulate pulse-like motions. Baker [7] developed a method to identify and extract pulses in near-fault ground motions by decomposing velocity time series into wavelets. He suggested that if the largest extracted velocity pulse in a ground motion is "large" enough compared to the remaining motion, the ground motion is classified as pulse-like, and the associated pseudo-period is regarded as the pulse period. Using the pulse-like motions identified by Baker [7], Champion and Liel [8] showed that buildings may have a substantially lower potential for collapse under pulse-like motions (especially when $T_s/T_P \leq 0.5$)) than under far-field motions. The results of their study indicated that this phenomenon is more prominent for ductile buildings.

While the above mentioned studies were restricted to fixed-base buildings, it is well known that soil-structure interaction (SSI) may have a pronounced effect on the seismic performance of buildings [9–13]. SSI can change the response of a building by altering the foundation input motion and the dynamic properties of the

interacting system. The former could even occur for massless foundations without the presence of any superstructure, referred to as the "kinematic interaction", where a stiff foundation cannot follow the pattern of free-field motion. The latter is a direct result of the "inertial interaction" where a shaking superstructure dissipates seismic energy into its foundation through soil deformation and wave radiation, which, in turn, affects the vibration of the structure. More recently, the effects of pulse-like motions on flexible-base structures have received considerable attention (e.g. [14–18]). Similar to the observations stated earlier for fixed-base structures, these studies in general showed a strong dependence of seismic response of flexible-base structures on the fundamental period of the interacting system T_{ssi} relative to the pulse period T_P [16,17].

Although much work has been devoted to the investigation of the effects of pulse-like records on fixed and flexible-base buildings, less effort has been made on the development of a comprehensive design framework that includes these effects [19,20]. Procedures for seismic design or assessment of flexible-base structures have been proposed by a number of researchers [21–25], but as yet few studies have introduced the combined SSI and pulse effects in the design process. SSI procedures in current seismic provisions and standards (e.g. [26,27]) for design of new buildings adopt a force-based approach, which does not address the effects of velocity pulses. This study attempts to incorporate, for the first time, the effects of near-fault pulse motion into a practical direct displacement-based design (DDBD) procedure for seismic design of flexible-base structures. Note that not all near-fault ground motions exhibit intensive velocity pulses, which are also not necessarily due to forward-directivity (depends on orientation of the site relative to the fault plane). The current work deals with near-fault impulsive motions without permanent ground displacements. The proposed design procedure is suitable for buildings supported by raft foundations that are bonded to a homogeneous soil half-space (i.e. for relatively heavy buildings on softer soils). Foundation input motion is assumed to be due to coherent vertically propagating shear waves, in which case kinematic interaction effects are not present. Soil nonlinearity is approximated using equivalent-linear shear modulus and damping ratio values that are compatible with the strain levels associated with the design scenario.

The paper is organised into five main parts (sections 2-6). Section 2 suggests a novel method to construct compatible design response spectra for near-fault earthquakes which accounts for the pulse period. Section 3 describes a practical approach for substituting an actual SSI system by an equivalent fixed-base single-degree-of-freedom (SDOF) oscillator. Section 4 integrates methods introduced in sections 2 and 3 into a DDBD framework considering both SSI and near-fault pulse effects. Two step-by-step design procedures based on, respectively, inelastic displacement spectra and equivalent linearisation are then presented in Section 4, with their effectiveness verified and compared using results of response history analysis for two design examples. Finally, the applicability of the proposed design methodology is discussed in Section 5 and conclusions are provided in Section 6.

2. DESIGN RESPONSE SPECTRUM

2.1 Bi-normalised response spectrum

Currently the seismic design of new structures (or evaluation of existing structures) is usually based on a design response spectrum, which is representative of the response of a series of SDOF oscillators subjected to an ensemble of ground motions. The design response spectrum can be determined empirically by averaging the individual response spectra corresponding to each ground motion in the ensemble with peak response parameters (i.e. acceleration, relative velocity or relative displacement) normalised by the corresponding peak ground values (i.e. peak ground acceleration (PGA), peak ground velocity (PGV) and peak ground displacement (PGD)). However, the response spectra of real earthquake records usually exhibit peaks at predominant periods (T_g) that may vary significantly from one record to another. For pulse-like motions, T_P is a predominant period around which spectral shapes can be significantly different from those without impulsive characteristics [19]. Previous studies showed that code-specified spectral shapes based on averaged spectra using various ground motion records failed to reflect realistic spectral ordinates around predominant periods, which may lead to non-conservative design solutions (e.g. reduced spectral accelerations due to irrational averaging) [28–32].

We may define T_{ga}, T_{gv} and T_{gd} as the predominant periods (T_g) at which the pseudo spectral acceleration (PSA), pseudo spectral relative velocity (PSV), and spectral relative displacement (SD) attain their maximum values, respectively. The spectral values are related to one another by the following relations [33]:

$$\mathrm{PSA} = \mathrm{PSV}\left(\frac{2\pi}{T}\right) = \mathrm{SD}\left(\frac{2\pi}{T}\right)^2 \tag{1}$$

where T is the natural period of the vibrating system. Normalising T by the stated predominant periods T_g has been shown to produce more realistic design spectra (referred to as the "bi-normalised spectra" [30]) than the conventional normalised response spectra for near-fault regions [28,29,31]. The idea of such an approach is to preserve the peaks that exist in the individual response spectra at the predominant period T_g. A common practice to develop a bi-normalised design response spectrum is to fit the design spectrum to the statistical mean spectrum through a least-square analysis. The mean spectrum is usually obtained using a large number of ground motion records with the stated normalisation methods [28–31]. For example, Maniatakis and Spyrakos [28] derived such a bi-normalised displacement response spectrum (i.e. SD/PGD vs. T/T_{gd}) as a more accurate means of estimating design displacement demands of structures located in near-fault regions, compared with the current code spectrum. However, as pointed out by Malhotra [34] and Xu *et al.* [35], the response spectrum of a real earthquake record usually only correlates well with PGA, PGV and PGD in the short, intermediate and long-period regions, respectively. In this sense, a bi-normalised displacement spectrum obtained by averaging SD/PGD for a large number of earthquake records may not be reliable for predicting the maximum displacement of short and intermediate-period structural systems (i.e. those with $T_s<T_{gd}$), which is crucial for direct displacement-based design procedures utilising displacement spectra.

It is a simple matter to show that the pseudo-acceleration calculated using the Maniatakis and Spyrakos [28] displacement spectrum tends to infinity for near-rigid systems, which is contradictory to the fact that the PSA of short-period systems should be close to PGA. A possible solution to the incompatibility between SD and PSA may be in using the Newmark-Hall spectrum [36] based on scaling spectral ordinates from PGA, PGV and PGD. The next subsection adopts the Newmark and Hall procedure to suggest new compatible design response spectra for near-fault sites that can efficiently retain the spectral peaks.

2.2 Compatible response spectrum

Figure 1(a) illustrates the suggested compatible design response spectrum constructed on a four-way logarithmic chart. Note that values of PSV, PSA and SD are read along the vertical, -45°, and +45° axes, respectively, on a log scale. The spectral ordinates at control points a-e are scaled from peak ground parameters by various amplification factors at the corresponding control periods T_a-T_e. It is assumed that PSA=PGA and SD=PGD for $T\leq T_a$ and $T\geq T_e$, respectively. Periods T_b, T_c and T_d correspond to the predominant periods T_{ga}, T_{gv} and T_{gd} at which peak ordinates of PSA, PSV and SD are scaled from PGA, PGV and PGD by amplification factors α_a, α_v and α_d, respectively. The design pseudo-velocity spectrum is constructed by connecting straight lines between the control points on the four-way logarithmic chart, while the pseudo-acceleration and the displacement spectra are derived from PSV using Equation (1).

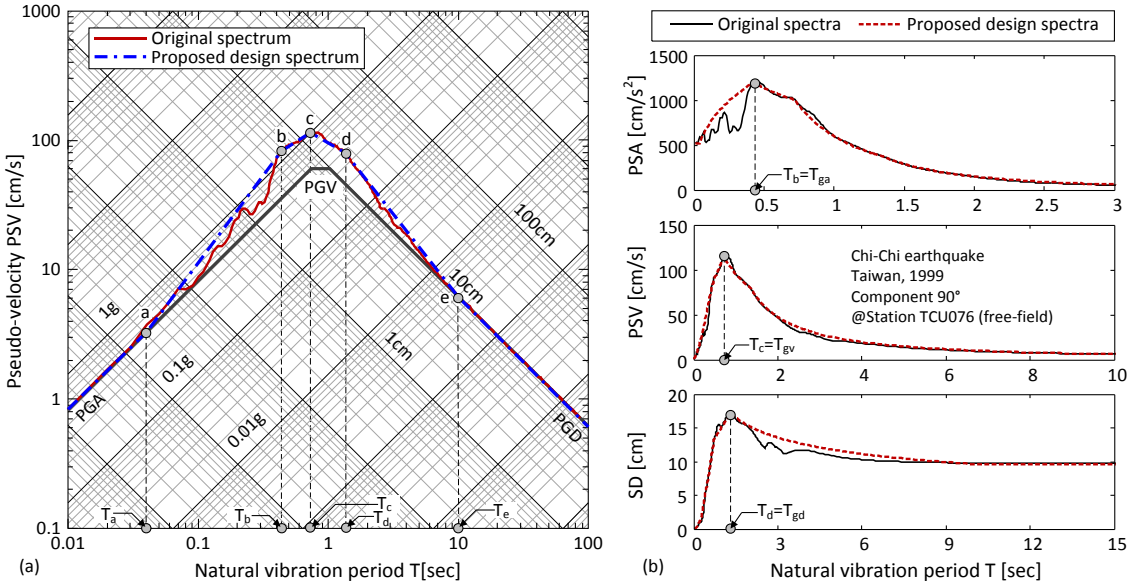

Figure 1. (a) Suggested design response spectrum plotted on tripartite logarithmic chart (example presented for Chi-Chi earthquake in 1999, considering a 5% damping ratio); and (b) comparisons of the proposed and the actual response spectra.

Figure 1(b) shows that the response spectra obtained using the proposed method compare well with the actual spectra. Particularly, the peak responses are very well captured by the proposed spectra. As will be shown in the next subsection, compared with the conventional Newmark-Hall spectrum [36], the new proposed design spectra explicitly take into account the pulse period T_P and can capture the spectral peaks that may vary significantly from one seismic event to another.

2.3 Construction of compatible design spectra

In order to apply the suggested compatible spectra in design practice, the values of peak ground motion (PGA, PGV and PGD), control periods (T_a-T_e) and spectral amplification factors (α_a, α_v and α_d) should be determined, as illustrated in Figure 2. For seismic design of structures in near-fault regions, the stated spectral parameters are mainly a function of the earthquake moment magnitude M_W, the closest distance to the fault rupture R, and the site soil condition (i.e. [29,37–39]). This section summarises empirical relations of the spectral parameters that were adopted to construct the design spectra in this study. These relations were developed by different researchers based on statistical analyses, and the mean values of the parameters in those analyses were used in this study unless stated otherwise. Note that the proposed displacement-based design methodology is general, and any design response spectrum can be easily adopted.

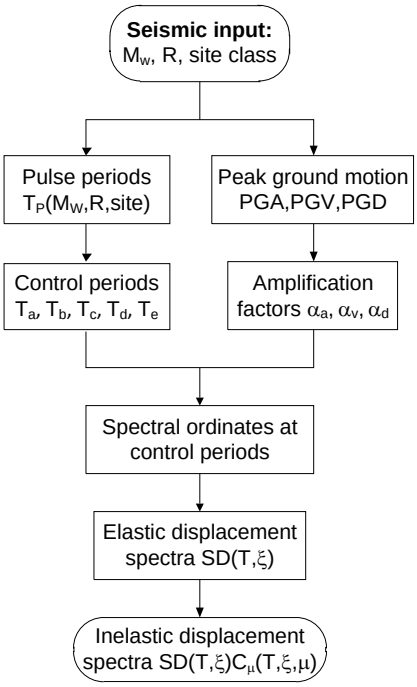

Figure 2. Schematic flowchart showing the construction of the design spectra.

2.3.1 Peak ground motion parameters

Due to the lack of prediction models for peak impulsive ground motion in the literature, the current study adopts the attenuation relationship developed by Tromans and Bommer [37]:

$$\log(\mathrm{PGP}) = C_1 + C_2 \mathrm{M_S} + C_4 \log\left(\sqrt{R^2 + h_0^2}\right) + C_\mathrm{A} S_\mathrm{A} + C_\mathrm{S} S_\mathrm{S} + \sigma P \tag{2}$$

where PGP is the peak ground motion parameter, i.e. PGA, PGV, PGD; M_S is the surface wave magnitude; S_A and S_S are variables relating to site soil condition; C_1, C_2, C_4, C_A, C_S and h_0 are coefficients provided in [37]; σ is the standard deviation (std) of log(PGP) while P equals zero and unity, respectively, for the mean and the mean+ std values of log(PGP). Note that the moment magnitude M_W and the surface wave magnitude M_S are interchangeable for $6 \leq M_S \leq 8$ (e.g. [40,41]), whereas for lower values of M_S, empirical relations can be used to convert M_S to M_W [42].

2.3.2 Control spectral periods

For near-fault pulse-like motions, the predominant periods at which spectral peaks occur have been shown to correlate well with the pulse period T_P. Therefore, a convenient way to determine the control periods is to link them to T_P, which is mainly a function of the earthquake magnitude (e.g. [7,19,29,39]):

$$\ln(T_\mathrm{P}) = X_1 + X_2 \mathrm{M_W} \tag{3}$$

The values of X_1 (-8.6 for rock sites and -5.6 for soil sites) and X_2 (1.32 for rock sites and 0.93 for soil sites) suggested by Bray and Rodriguez-Marek [39] were used here to determine T_P. It has been shown that the predominant period for PSV (i.e. T_{gv}=T_c), in most cases is lower than the pulse period T_P [7,43]. Therefore, T_{gv} was reduced from T_P through factors of 0.78 and 0.93 for rock and soil sites, respectively, as suggested by Xu *et al.* [43]. In this study, the spectral predominant period for SD, T_{gd}, was considered to be equal to the pulse period T_P according to Maniatakis and Spyrakos [28]. The spectral predominant period T_{ga} for PSA (T_b in Figure 1) was estimated using the empirical expression proposed by Rathje *et al.* [38]:

$$T_{ga} = Y_1 + Y_2(M_W - 6) + Y_3 R \tag{4}$$

where coefficients Y_1 to Y_3 are dependent on the site condition. The control periods T_a and T_e were assumed to be $0.004T_P$ and $10T_P$, respectively, which are in accordance with those suggested in Mavroeidis *et al.* [29]. It should be mentioned that the suggested design spectrum is close to the one proposed by Mavroeidis *et al.* [29] based on a statistical analysis of bi-normalised pseudo-velocity spectra (PSV/PGV vs. T/T_P) obtained from the records of 20 seismic events. However, unlike the Mavroeidis *et al.* [29] spectra whose control periods (normalised by T_P) were determined by matching their design spectra to the mean bi-normalised pseudo-velocity spectra obtained from the statistical analysis, T_b-T_d in the present study have clear physical meanings as they correspond to spectral peaks.

Figure 3 shows that the adopted spectral predominant periods proposed in the aforementioned studies (highlighted by dashed lines) are generally in the same range as the control periods suggested by Mavroeidis *et al.* [29] (highlighted by solid lines and shaded areas). However, as discussed earlier, the control periods (T_b-T_d) in Mavroeidis *et al.* [29] were determined from the averaged bi-normalised PSV and may not correspond to the actual spectral peaks.

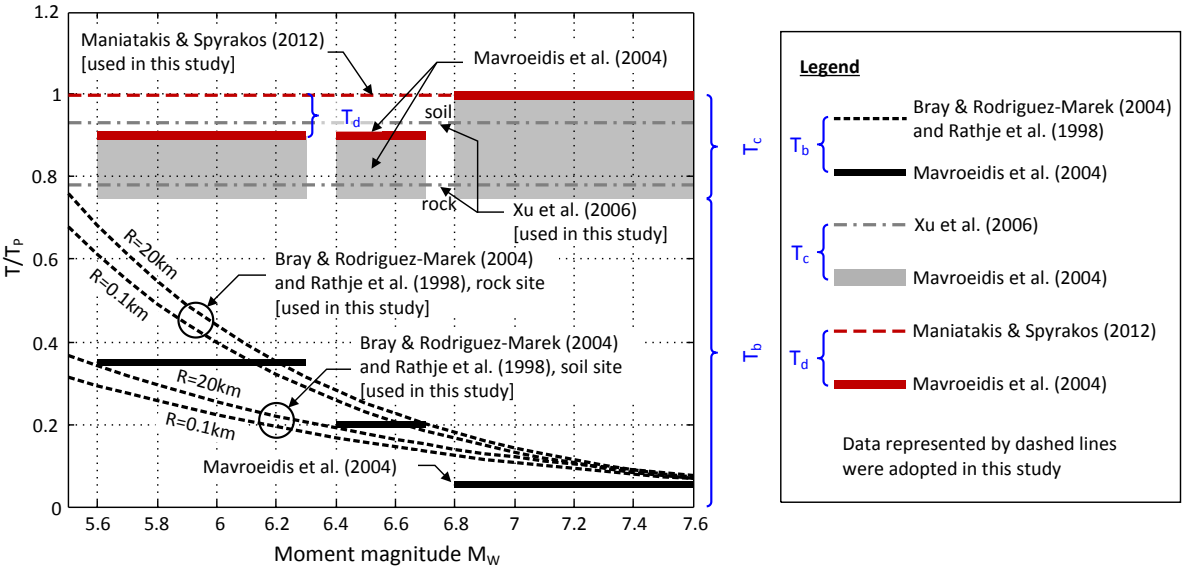

Figure 3. Variation of the normalised control periods (T_b/T_P, T_c/T_P and T_d/T_P) with earthquake magnitude M_W, closest distance to fault rupture plane R, and site condition.

2.3.3 Spectral amplification factors

Spectral amplification factors are required to scale peak ground parameters at the corresponding control periods. Since increasing damping reduces peak structural responses, these factors should also be a function of damping ratio ξ, as shown in Equation (5).

$$\alpha_i(T_{gi},\xi) = \alpha_i(T_{gi},5\%)/B_d(T_{gi},\xi) \tag{5}$$

where i=a, v and d represent quantities associated with PSA, PSV and SD, respectively. In this study, the values of $\alpha_a(T_{ga},5\%)$, $\alpha_v(T_{gv},5\%)$ and $\alpha_d(T_{gd},5\%)$ were taken as 3.5, 2.8 and 2.4, respectively, according to references [28,30,31]. The term B_d is a damping correction factor defined as:

$$B_d(T_{gi},\xi) = \frac{SD(T_{gd},5\%)}{SD(T_{gd},\xi)} = \frac{PSV(T_{gv},5\%)}{PSV(T_{gv},\xi)} = \frac{PSA(T_{ga},5\%)}{PSA(T_{ga},\xi)} \tag{6}$$

For near-fault earthquake motions, Hubbard and Mavroeidis [44] suggested damping correction factors that explicitly include the effect of the pulse period T_P. However, these factors may significantly underestimate B_d for

$T/T_P \leq 0.5$ that coincides with the range of T_b/T_P for soil sites [44]. Therefore, in this study the expression of B_d proposed by Hatzigeorgiou [45] for near-fault motion was used:

$$B_d(T,\zeta) = \left\{1 + (\zeta - 5)\cdot\left[1 - 0.30\ln(\zeta) + 0.02(\ln(\zeta))^2\right]\cdot\left[-0.09 + 0.01\ln(T) + 0.01(\ln(T))^2\right]\right\}^{-1} \quad (7)$$

where $\zeta=100\xi$ is the damping ratio in percentage. Figure 4 illustrates the pseudo-acceleration and displacement spectra derived using the suggested procedure for structures located on a soil site one kilometre away from the rupture fault of an M_W 6.5 earthquake.

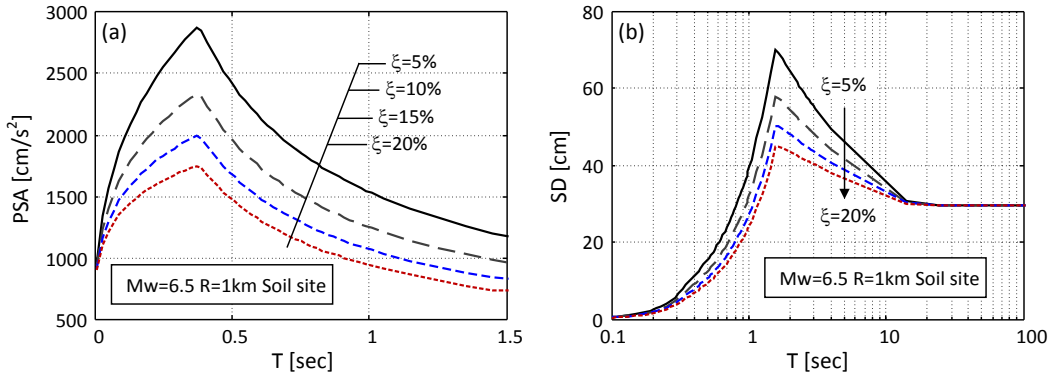

Figure 4. Proposed response spectra for various damping ratios: (a) pseudo-acceleration spectra and (b) displacement spectra.

2.3.4 Inelastic design spectra

Inelastic design response spectra can be developed by applying modification factors to their elastic counterparts. For example, the inelastic spectral acceleration values be obtained by dividing their elastic values by a ductility reduction factor R_μ for given ductility ratios of μ. The inelastic displacement spectrum can be calculated by multiplying the corresponding elastic SD by an inelastic displacement ratio C_μ, which equals μ/R_μ for an elastic-perfectly plastic restoring force-deformation hysteretic behaviour. Qu *et al.* [46] evaluated the accuracy of several empirical relations for R_μ and demonstrated that the following expression proposed by Ordaz and Pérez-Rocha [47] was the most suitable model for near-fault motions:

$$R_\mu = 1 + \left(\frac{\mathrm{SD}(T,\xi,\mu=1)}{\mathrm{PGD}}\right)^{\beta}(\mu-1), \quad \beta = 0.388(\mu-1)^{0.173} \quad (8)$$

Applying Equations (8) to the 5% damped displacement spectrum in Figure 4(b), the corresponding ductility reduction factors and inelastic displacement ratios are presented in Figure 5. Note that the peaks and valleys respectively in R_μ and C_μ spectra occur at the pulse period T_P, which agrees with the results in references [48–50]. It is worth mentioning that the inelastic spectra constructed by the suggested procedure are compatible with their original design elastic spectra, since the modification factors R_μ and C_μ are functions of SD. As a result, the dependence of the inelastic spectra on damping is automatically accounted for by using the damping-dependent SD. This is in sharp contrast to the common inelastic spectra (usually for 5% damping) constructed using smooth R_μ and C_μ spectra that may be incompatible with the design elastic spectra, as indicated by Fajfar [51].

It should be noted that the compatible spectrum described in this section was constructed using existing empirical prediction models for ground motions and spectral shapes. While the suggested procedure is conceptually a better alternative to the conventional bi-normalised response spectra, there are limitations to the proposed compatible response spectrum, which are discussed in detail in Section 5.

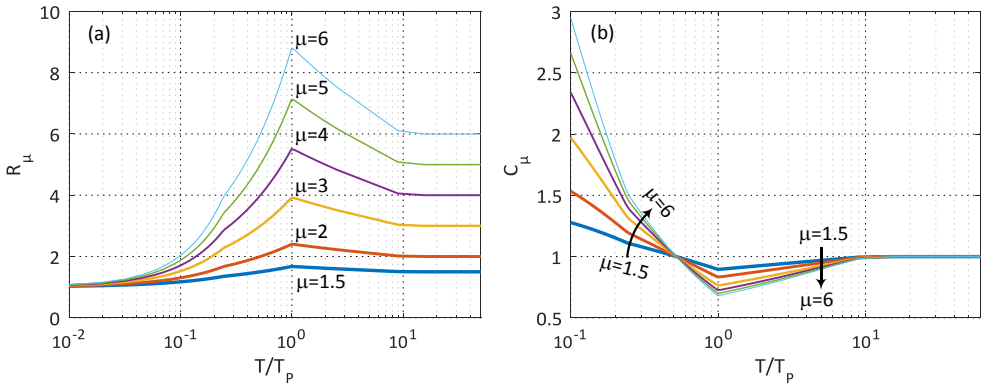

Figure 5. Constant-ductility spectra (5% damping) obtained using Equations (10) and (11) with SD in Figure 4(b): (a) ductility reduction factors and (b) inelastic displacement ratios.

3. SOIL-STRUCTURE INTERACTION

3.1 SSI in current seismic design standards and provisions

While current seismic standards and provisions for evaluation and retrofit of existing buildings mainly adopt a displacement-based approach for SSI analyses [52,53], conventional seismic design codes used for design of new buildings are still force-based [26,27]. In the ASCE 7-16 [27] suggested design method, the superstructure is substituted by an SDOF oscillator representing its fundamental mode of vibration and the foundation system is replaced by equivalent sway and rocking springs as shown in Figure 6(a). The effect of structural yielding is taken into account by reducing the elastic base shear using the response modification coefficient R_μ which is based on the behaviour of an elastic-perfectly plastic fixed-base model. The effects of soil-structure interaction are accounted for by imposing a further reduction to the design base shear of the yielding structure in accordance with a period lengthening ratio λ and a system damping ratio ξ_{ssi} given by:

$$\xi_{ssi} = \lambda_{eq}^{-3}\xi_s + \left(1-\lambda^{-2}\right)\xi_g + \xi_r \tag{9}$$

where ξ_s is the structural linear viscous damping ratio, ξ_g is the soil hysteretic damping ratio and ξ_r is the contribution of foundation radiation damping. The period lengthening ratios are calculated by:

$$\lambda_{eq} = \frac{T_{ssi,eq}}{T_{s,eq}} = \sqrt{1+\frac{1}{\mu_s}\left(\lambda^2-1\right)} \tag{10}$$

$$\lambda = \frac{T_{ssi}}{T_s} = \sqrt{1+\frac{k_s}{k_h}+\frac{k_s H^2}{k_\theta}} \tag{11}$$

where H is the height of the SDOF superstructure; and k_s, k_h, and k_θ are stiffness coefficients corresponding to the lateral displacement of the superstructure, and foundation swaying and rocking motions, respectively. Subscripts "s" and "ssi" are used to represent quantities associated with the fixed-base structure and the SSI system, respectively (see Figures 6(a)-(b)), whereas the subscript "eq" denotes quantities of the equivalent as shown in Figure 6(c).

An issue with the stated procedures is that the strength reduction due to structural yielding was treated independently without considering SSI effects, which, may lead to non-conservative results [10,25]. Although ASCE 7-16 [27] provides an upper bound reduction for the design base shear, the resulting design solutions can still be unsafe [54]. Compared to the conventional force-based design philosophy, the direct displacement-based design (DDBD) has been shown as a more rational approach, since it uses displacement demands (which are directly related to structural and non-structural damage) as the main design parameters [55]. However, it is challenging to directly use Equation (9) in a displacement-based SSI design procedure since the radiation damping term ξ_r is frequency-dependent. This means that calculation of ξ_{ssi} requires the knowledge of elastic fundamental periods of both the superstructure T_s and the SSI system T_{ssi}, which are two unknowns that need to be determined, as opposed to a force-based design (or a displacement-based evaluation) procedure that starts from a known value of initial period. The following subsection presents the proposed equivalent fixed-base SDOF (EFSDOF) oscillators that are suitable for displacement-based design of flexible-based structures.

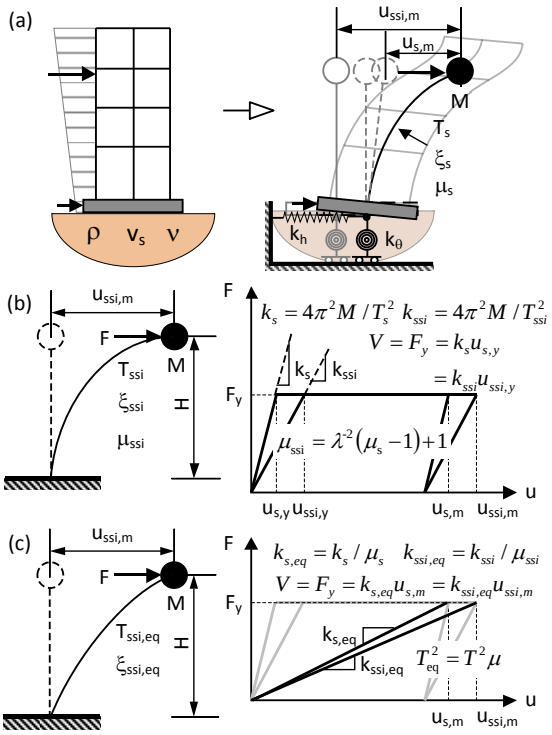

Figure 6. Simplified SSI models: (a) Sway-rocking model, (b) nonlinear EFSDOF oscillator, and (c) linear EFSDOF oscillator.

3.2 EFSDOF oscillators

This study is focused on surface foundations (having an equivalent radius r) that are assumed to be rigid and bonded to a homogeneous soil half-space (i.e. for relatively heavy buildings on softer soils) having an effective shear wave velocity v_s, a mass density ρ, and a Poisson's ratio ν of 0.4 for preliminary design purposes [53]. In order to facilitate design process, a number of dimensionless design parameters are introduced, including structure-to-soil stiffness ratio $a_0=2\pi H/(T_s v_s)$, slenderness ratio of the building $s=H/r$, and structure-to-soil mass ratio $\bar{m}=M/(\rho H r^2)$ with M being the mass of the SDOF superstructure which is ten times that of the foundation [53].

An SSI system can be replaced by either a nonlinear EFSDOF oscillator (Figure 6(b)), characterised by T_{ssi}, ξ_{ssi}, and μ_{ssi}, or a linear EFSDOF oscillator (Figure 6(c)) having a period of $T_{ssi,eq}$ and an equivalent viscous damping ratio of $\xi_{ssi,eq}$ encapsulating energy dissipation by all mechanisms that occur upon the expected degraded state of the system. Both oscillators share the identical T_{ssi} and ξ_{ssi} when the SSI systems they represent are purely elastic. Using the dimensionless parameters, Equation (11) can be written as:

$$\lambda = \frac{T_{ssi}}{T_s} = \sqrt{1 + \left(\frac{1}{5\eta_h s} + \frac{9s}{40\eta_\theta}\right) a_0^2 \bar{m}} \tag{12}$$

where η_h and η_θ are dynamic modification factors for k_h and k_θ, respectively, associated with the equivalent natural frequency of the system T_{ssi} as follows [57]:

$$\eta_h = 1 - 0.62\gamma\chi, \quad \eta_\theta = 1 - \frac{0.327\psi + 0.278\gamma\chi + 0.013\gamma^2}{\psi + 1.6\chi\gamma + 0.64\gamma^2}\gamma^2 \tag{13}$$
$$\gamma = \frac{2\pi r}{T_{ssi} v_s}, \quad \chi = \sqrt{\frac{\psi - 1}{2}}, \quad \psi = \sqrt{1 + 4\xi_g^2}$$

Note that T_{ssi} exists on both sides of Equation (12) and can be solved iteratively.

Following Equation (9), the elastic system damping ratio ξ_{ssi} takes the following functional form:

$$\xi_{ssi} = \lambda^{-3}\xi_s + (\lambda^2 - 1)\xi_g + \xi_r \tag{14}$$

where ξ_r can be approximated using the following closed-form expressions:

$$\xi_r = (1 - \lambda^{-2})^{1.5} \bar{m}^{-0.5} / f(s, \bar{m}), \; f(s, \bar{m}) = [0.38\ln(\bar{m}) + 1.42]s^{3.5} + \ln(2s)(\bar{m} + 0.8) + 1.3 \tag{15}$$

where $f(s,\bar{m})$ was derived in this study through a least-square analysis against the results of the exact solution developed by Maravas *et al.* [56] obtained iteratively using the Veletsos and Verbič impedance functions [57]. Equation (15) takes into account the frequency-dependent nature of radiation damping and is valid for common building structures with $0.3 \le \bar{m} \le 0.7$ and $0.5 \le s \le 4$. Figure 7 compares the foundation radiation damping ratios calculated by the proposed closed-form expression and the exact solutions for systems with different structure-to-soil mass and slenderness ratios. It is shown that despite some slight underestimation of ξ_r for $s \le 1$ (conservative in design), the proposed closed-form expression is sufficiently accurate for design purposes.

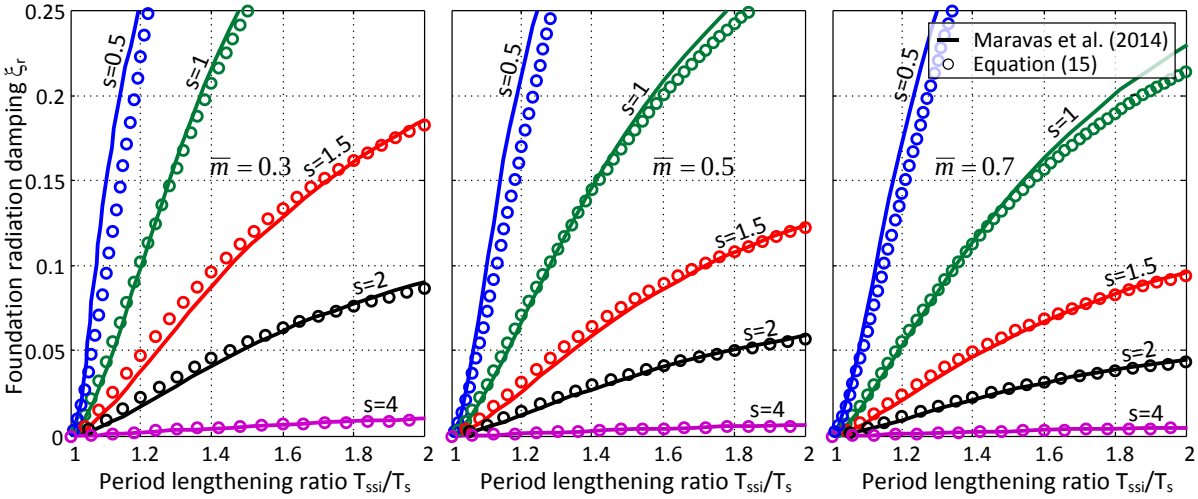

Figure 7. Comparison of the foundation radiation damping ratio calculated by the proposed closed-form expression and the exact solutions.

While the soil material damping (hysteretic dissipation of energy) is strain-dependent, it has been shown to be insensitive to the frequency of vibration [58]. The strain-dependent shear modulus degradation and damping curves serve as the basis for the equivalent-linear method for site response analysis. The two curves are related to each other by the following expression [59]:

$$\xi_g = \frac{1+\exp\left(-0.0145\mathrm{PI}^{1.3}\right)}{6}\left[0.586\left(\frac{G}{G_0}\right)^2 - 1.547\frac{G}{G_0} + 1\right] \tag{16}$$

where PI is the plasticity index in percentage, G is the effective soil shear modulus equal to ρv_s^2, and G_0 is the low-strain shear modulus that can be evaluated using the corresponding shear wave velocity v_{s0}. The shear modulus degradation ratio G/G_0 is related to peak spectral acceleration and site classes in Table 19.3-2 of ASCE 7-16 [27].

For the nonlinear EFSDOF oscillator, an effective ductility ratio is used to measure the degree of inelasticity of the SSI system (Figure 6(b)):

$$\mu_{ssi} = \lambda^{-2}\left(\mu_s - 1\right) + 1 \tag{17}$$

whereas the equivalent viscous damping ratio of the linear EFSDOF oscillator can be obtained by applying standard equivalent linearisation methods on the nonlinear model in Figure 6(b). Based on well-known Gulkan and Sozen methods for reinforced concrete (RC) frame structures [60], Moghaddasi et al. [24] suggested the following expression to evaluate the equivalent damping ratio of EFSDOF systems:

$$\xi_{ssi,eq} = \xi_{ssi}\left(\lambda_{eq}\right) + \frac{1 - 1/\sqrt{\mu_{ssi}}}{\pi} \tag{18}$$

It should be noted that, in general, the equivalent viscous damping ratio values for RC and steel frame buildings are close when having similar ductility demands [55]. However, designers can use other appropriate expressions to estimate the equivalent viscous damping ratio in accordance with the structural system of interest.

4. DIRECT DISPLACEMENT-BASED DESIGN METHODOLOGY FOR FLEXIBLE-BASE BUILDINGS

A controversial issue regarding the DDBD approach is the use of heavily damped elastic spectra for estimating inelastic displacement demands of SDOF systems, on the basis of an equivalent linear approximation of the actual nonlinear behaviour. Previous research has suggested that, instead of using elastic spectra with equivalent viscous damping, inelastic design spectra could be adopted for estimating inelastic displacement demands with

higher accuracy [51,61,62]. This section presents a procedure for soil-structure interaction analysis within the framework of the DDBD approach, as illustrated in Figure 8. The effectiveness of both equivalent linearisation and inelastic spectra methods is assessed by means of two design examples.

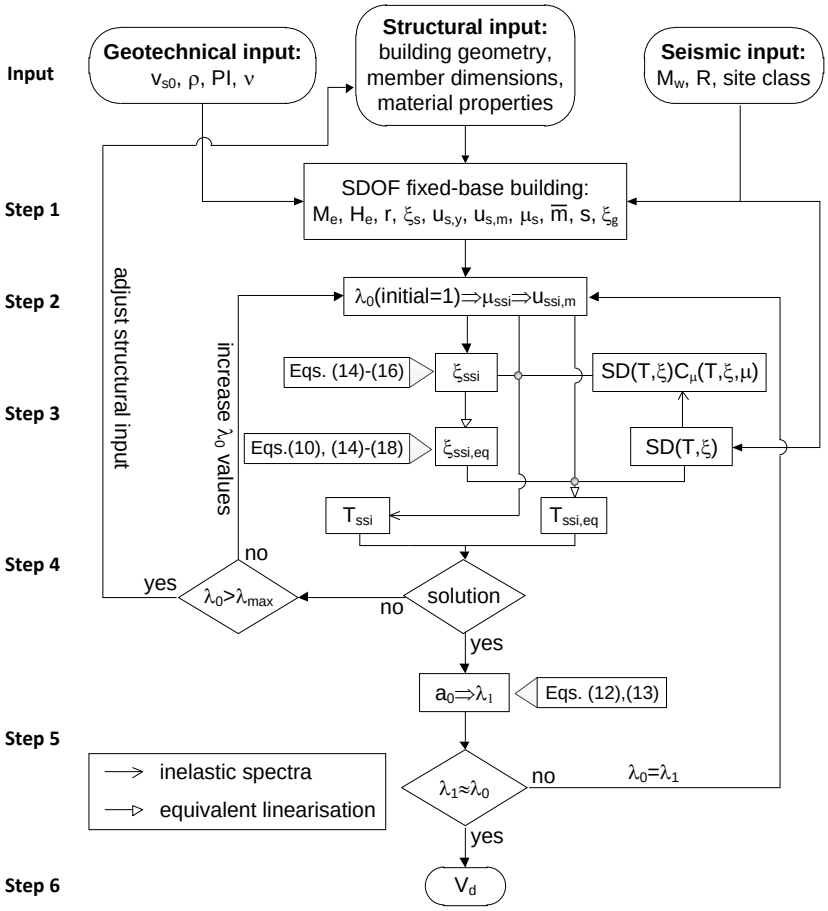

Figure 8. Flowchart illustrating the overall DDBD process for flexible-base yielding structures.

4.1 Design procedure based on inelastic spectra

The suggested design procedure for flexible-base buildings subjected to near-fault pulse-like motions involves the following steps, in accordance with Figure 6(b) and Figure 8:

1. SDOF representation of the design building
   Determine the properties of the fixed-base building corresponding to its inelastic first-mode shape (assumed similar to its elastic shape [55]) and the structural ductility, slenderness and mass ratios.
2. Design displacement of the EFSDOF oscillator $u_{ssi,m}$
   Calculate the yield displacement and the effective ductility ratio of the nonlinear EFSDOF oscillator, obtain the design displacement $u_{ssi,m}$. For the 1st iteration, $\lambda_0=T_{ssi}/T_s$ can be assumed to be equal to 1 (i.e. fixed-base condition).
3. System damping ratio ξ_{ssi}
   Calculate the system damping ratio ξ_{ssi} using λ_0.
4. Equivalent natural period T_{ssi}
   Construct the inelastic displacement spectrum using $SD(T, \xi_{ssi},\mu_{ssi})=SD(T,\xi_{ssi})\cdot C_{\mu,ssi}(T,\xi_{ssi},\mu_{ssi})$ following the procedures described in Section 2. Determine T_{ssi} that corresponds to $u_{ssi,m}$. If no solution is found, i.e. $u_{ssi,m}>\max[SD(T, \xi_{ssi},\mu_{ssi})]$, increase λ_0 values and repeat steps 2-4 until solutions found. If $\lambda_0>\lambda_{max}$ (say, 5), adjust structural geometry or member dimensions and repeat steps 1-4 until solutions found.
5. Check convergence of design solution
   Calculate T_s and a_0 to evaluate a new value of λ_1. If λ_1 is close to λ_0 within an acceptable tolerance, proceed to step 6. Otherwise, let $\lambda_0=\lambda_1$ and repeat steps 2 to 5 until a satisfactory tolerance of λ is obtained.
6. Design base shear V_d
   Determine the design base shear strength V_d which is then distributed to each floor to design structural members.

4.2 Design procedure based on equivalent linearisation

The second procedure adopts elastic design spectra derived for high damping ratio values to account for structural inelasticity, in accordance with Figure 6(c) and Figure 8. Steps 1, 2, 5, and 6 in the inelastic spectra method (subsection 4.1) remain unchanged here whereas steps 3, 4 are modified as follows.

3. Equivalent linear viscous damping ratio $\xi_{ssi,eq}$
   Estimate the effective period lengthening ratio $\xi_{ssi,eq}$ using λ_{eq} and μ_{ssi}
4. Equivalent period of the yielding system $T_{ssi,eq}$
   Construct the design elastic displacement spectrum $SD(T,\xi_{ssi,eq})$ following the procedures described in Section 2. Obtain $T_{ssi,eq}$ corresponding to $u_{ssi,m}$ on the spectum. The solution process is the same as that in step 4 for the inelastic spectra method.

4.3 Design examples

The effectiveness of the suggested direct displacement-based procedure is demonstrated using two example SDOF structures. The properties of the SDOF structures were extracted from two framed buildings of which the detailed design was originally presented in references [55,63] for the fixed-base condition. The first example Ex.1 relates to a steel building (Figure A1(a)) where the seismic resistance is provided by peripheral and interior resisting frames, while the second example Ex.2 represents a hybrid precast prestressed frame building (Figure A1(b)). Both structural systems are supported by a raft foundation constructed on a clay site two kilometres away from the rupture plane of the governing fault. The buildings were designed for a maximum drift ratio of 0.025 during an M_W 6.6 seismic event considering that the ground velocity motions at the site exhibit strong pulses (pulse-like ground motions).

Table 1 lists the properties of the design examples (calculated according to reference [55]) and the foundation soil. Tables A1-A4 within Appendix A summarise results of the iterative direct-displacement design procedures, based on both the inelastic spectra (subsection 4.1) and the equivalent linearisation (subsection 4.2) methods, for examples Ex.1 and Ex.2.

Table 1. Input structural and geotechnical parameters for the design examples

Parameter	Ex.1	Ex.2
Effective mass, M_e (tonnes)	2595	1965
Effective height, H_e (m)	12.24	14.43
Structural yielding displacement, $u_{s,y}$ (m)	0.183	0.043
Structural displacement demand, $u_{s,m}$ (m)	0.256	0.303
Structural ductility ratio, μ_s	1.4	7.0
Structural linear damping ratio, ξ_s	0.05	0.05
Low-strain shear wave velocity, v_{s0} (m/s)	240	240
Soil mass density, ρ (kg/m^3)	1800	1800
Plasticity Index, PI (%)	30	30
Soil Poisson's ratio, ν	0.4	0.4
Structure-to-soil mass ratio, $\bar{m}$	0.51	0.38
Slenderness ratio, s	0.81	1.02

The data in Tables A1-A4 show that for the building designed with a low ductility capacity in Ex.1, using elastic and inelastic spectra has led to similar design base shear values (i.e. V_d=22179 and 23335kN for the inelastic and equivalent linearisation methods, respectively). On the contrary, for the building designed with a high ductility capacity in Ex.2, using the equivalent linearisation method resulted in a design base shear which is more than two times greater than that obtained using the inelastic spectra method. The adequacy of these two design solutions is studied in the next subsection using nonlinear response history analysis.

4.4 Verification using response history analysis

Since the design scenario involves pulse-like ground motions, 91 fault-normal pulse motions identified by Baker [7] were processed for the verification analyses in this study. These records were firstly modified using the RSPMatch09 program [64] to match the design pseudo-acceleration response spectrum (5% damping ratio).

RSPMatch09 performs time-domain spectral matching by adding adjustment wavelets to an initial acceleration time series. The model 7 tapered cosine function recommended by RSPMatch09 was adopted for the spectral matching to prevent drift in the modified velocity and displacement time series while preserving the non-stationary characteristics of the ground motion. Recognising that adding the wavelets to the original records may change their pulse-like characteristics, the modified motions were then filtered using the pulse-motion identification algorithm proposed by Baker [7] and the pulse periods calculated, i.e. the motion was identified as being "pulse-like" if the pulse indicator value was higher than 0.85. Following this criterion, sixteen spectrum-compatible pulse-like motions were selected as representative of the design ground motions for the nonlinear dynamic analysis. Figure B1 in Appendix B shows the strong velocity pulses in the modified ground motions. Comparison of the individual and mean values of the pulse periods of the design pulse-like motions with the design target values are presented in Figure 9, demonstrating a good agreement between the mean design motion and the target design scenario.

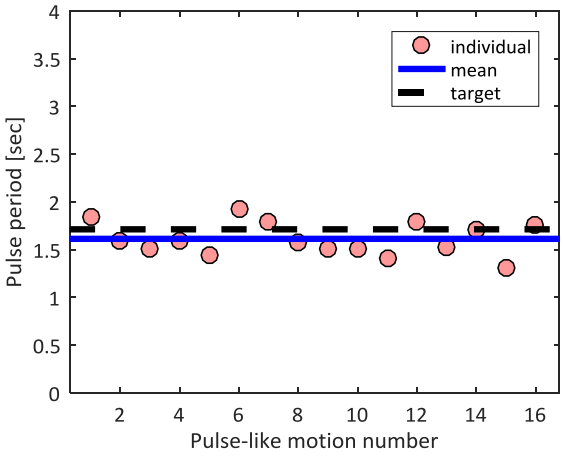

Figure 9. Pules periods of the design ground velocity motions compared with the target design value.

The superstructures were modelled by an SDOF oscillator having a mass of M_e, a height of H_e and elastic-perfectly plastic lateral force-displacement behaviour with a viscous damping ratio of 0.05. The dynamic behaviour of the raft foundation was simulated using a discrete-element model, which is based on the idealisation of a homogeneous soil under a rigid circular base mat as a semi-infinite truncated cone. More information about the flexible-base SDOF oscillators used to represent the actual soil-building interaction systems in this study is provided in reference [25].

Figure 10 compares the displacement demands of the flexible-base SDOF oscillators obtained from time-history analysis with the design target values listed in Tables A1 and A2 for Ex1 which was designed to undergo small inelastic deformations. Note that these displacements are defined relative to the ground and include the contributions of the foundation motions. The Ex 1 representative SDOF structures designed using either the inelastic spectra or the equivalent linearisation method experienced similar maximum displacements when subjected to the design pulse-like motions. This is consistent with the fact that the design base shear values using these two methods were fairly close.

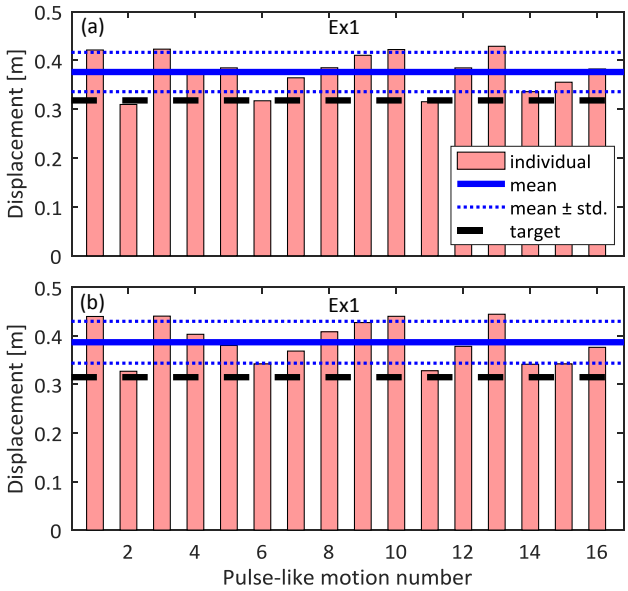

Figure 10. Displacement demands obtained from nonlinear response history analysis vs. target design values for Ex 1: (a) equivalent linearisation and (b) inelastic spectra methods.

For the structure in Ex.2 that was expected to dissipate a great amount of seismic energy through significant inelastic deformations, Figure 11 shows that the inelastic spectra method provides a noticeably better result, leading, on average, to a 7.9% higher displacement demand compared to the design displacement, while the mean value corresponding to the equivalent linearisation method is more than 40% lower than the target values (all individual values are also lower than the design displacement value).

Although using an inelastic design spectrum has been shown to be more efficient for seismic design of highly ductile fixed-base structures compared to using a heavily damped elastic spectrum [51,61,62], the authors by no means imply that inelastic spectra should always be favourable to elastic spectra in displacement–based design of flexible-base structures. In fact, both techniques are alternative tools in DDBD methods that need improvements (especially for pulse-like ground motions), and the performance of these techniques is affected by the procedures used for developing the design spectra and/or the methods used for the equivalent linearisation.

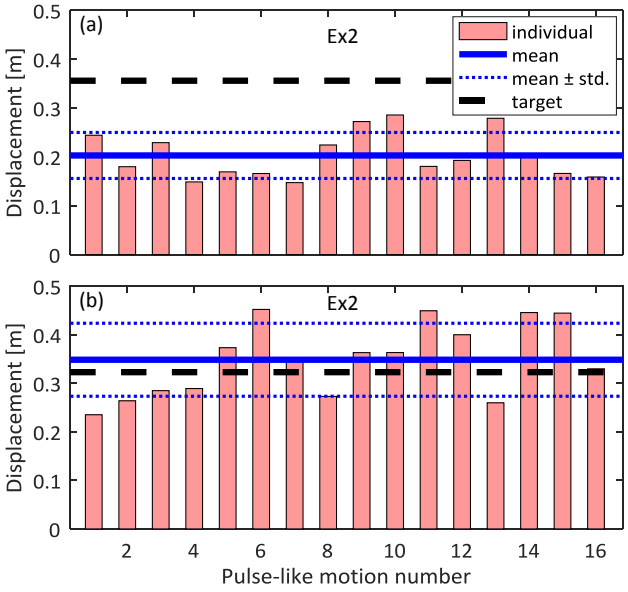

Figure 11. Displacement demands obtained from nonlinear response history analysis vs. target design values for Ex 2: (a) equivalent linearisation and (b) inelastic spectra methods.

While the focus of this study is on flexible-base structures, it is interesting to examine the response of corresponding fixed-base structures as well. Two additional scenarios were considered where structures were designed with a fixed-base assumption. Three cases are compared, defined as:

- Case 1- structures designed using the "fixed-base" assumption, supported on a rigid base and subjected to the sixteen pulse-like motions;
- Case 2- structures designed using the "fixed-base" assumption, supported on a flexible base and subjected to the sixteen pulse-like motions;
- Case 3- structures designed using the "flexible-base" assumption, supported on a flexible base and subjected to the sixteen pulse-like motions (results shown in Figures 10 and 11).

Note that the design process and solutions for the structures in case 3 are presented in Appendix A. The soil conditions for the case 2 structures were assumed to be identical to those in case 3, as presented in Table 1. Table 2 summarises the dynamic properties and design base shear values of the example structures designed according to the fixed and flexible-base assumptions.

The seismic response of the structures designed based on all three cases are compared in Figures 12 and 13. The displacement demands of SSI systems in cases 2 and 3 include the rigid-body movements of the foundation, whereas for case 1 the displacement demands correspond to the maximum structural distortion. In addition to evaluating the displacement demands against the target design values, the results of structural ductility demands are also compared in order to check if the actual structural inelasticity level is close to the design level. The comparison of the mean and target values for cases 1 and 3 is used to assess the effectiveness of the DDBD procedure; while for case 2, it displays the difference of the actual response of flexible-base structures designed using the fixed-base assumption and the target performance.

In general, the results of cases 1 and 3 (shown in Figures 12 and 13) indicate that using inelastic spectra is more effective than using elastic spectra in DDBD design of structures with and without considering soil-structure interaction, especially for structures designed to have higher ductility demands. It is also shown that the dispersion of the data is higher for structures with SSI-based design than for those designed using the fixed-base condition, and this dispersion increases with increasing target ductility demand. Figure 12(a) shows that the mean values of the displacement demand of Ex 1 structures in cases 1 and 2 are very close, suggesting that soil-structure interaction seems to have a negligible effect on their structural response. However, as illustrated in Figure 12(b), the structures with a flexible base in case 2 exhibited a much lower ductility demand compared to those in case 1 (lower than the target values). In fact, it seems that in this example the reduction of structural deformation (reduced ductility demand) and the increase in the foundation motion due to SSI cancelled each other out, leading to a similar displacement demand to the fixed-base structures.

Table 2. Design solutions for structures in cases 1, 2, and 3

Description	Case 1		Case 2		Case 3	
Base condition	Fixed base		Fixed base		Flexible base	
Simulation assumption	Fixed base		Flexible base		Flexible base	
Ex 1	EL[1]	IS[2]	EL	IS	EL	IS
T_s (sec)	0.667	0.682	0.667	0.682	0.896	0.919
a_0	0	0	1.268	1.468	1.118	1.090
V_d (kN)	42020	40228	42020	40228	23335	22179
Ex 2	EL	IS	EL	IS	EL	IS
T_s (sec)	0.447	0.760	0.447	0.760	0.505	0.781
a_0	0	0	0.997	1.554	2.339	1.510
V_d (kN)	16787	5819	16787	5819	13180	5501

Note: 1-EL=Equivalent Linearisation, 2-IS=Inelastic Spectra

Figure 13 compares the displacement and structural ductility demands of the Ex 2 structures in all three cases with the target values. It is shown that the SSI effect is insignificant for structures designed using inelastic spectra with high ductility demand. In this case, both fixed-base and SSI-based DDBD design methods lead to a practically identical design solution (see Table 2). This observation is in agreement with the results presented in Lu *et al.* [25], where the period elongation and damping due to foundation soil were negligible compared to those due to high levels of structural inelasticity; the overall response of the SSI system was governed by its highly nonlinear superstructure. On the other hand, the Ex 2 structures designed using heavily damped elastic

spectra (equivalent linearisation) exhibited very different seismic performances compared to those designed using inelastic spectra, which implies that these design solutions were not appropriate.

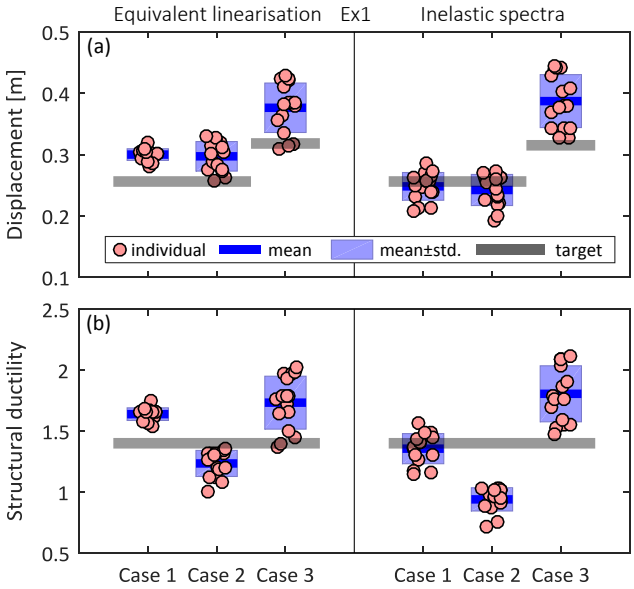

Figure 12. Results of nonlinear response history analysis vs. target design values for Ex 1 in all three cases: (a) displacement demands and (b) structural ductility demands.

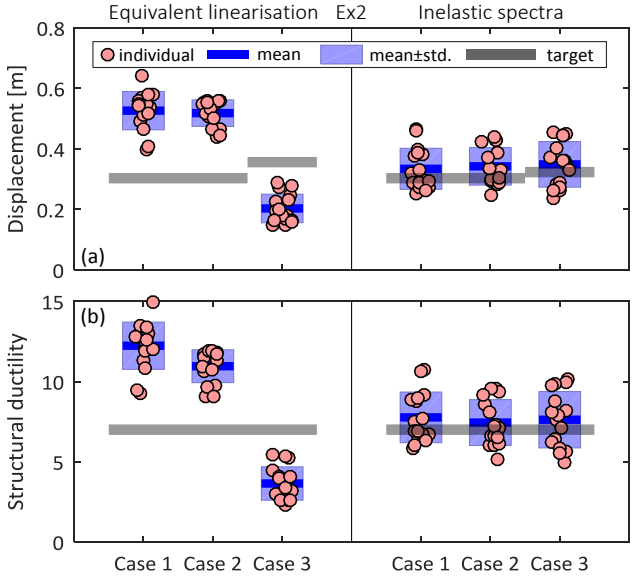

Figure 13. Results of nonlinear response history analysis vs. target design values for Ex 2 in all three cases: (a) displacement demands and (b) structural ductility demands.

5. POTENTIAL APPLICATIONS AND LIMITATIONS

The proposed design procedure is best suited to buildings supported by raft foundations. The effects of nonlinearity at the foundation-soil interface (e.g. foundation uplift and/or sliding), full mobilisation of foundation bearing capacity, soil inhomogeneity and foundation embedment were not considered. However, these effects can also be incorporated into the developed design framework by modifying the current procedure based on relevant references [21,22,65,66].

In the proposed design approach, the building was simplified as an SDOF structure based on its fixed-base fundamental mode of vibration and first mode-shape. While the SSI higher mode effects were not directly considered, recent research has shown that short-period velocity pulses can amplify the higher-mode (high-frequency) response of flexible-base buildings and affect their inter-storey drift distribution with respect to the

pulse periods [67,68]. Therefore, further studies should be conducted to quantify the alteration of higher-modes due to SSI so that more appropriate modifications can be applied to the basic procedure proposed in the current research.

It should be noted that the pulse-like motions may not necessarily be due to forward-directivity. The compatible response spectra suggested in this study were constructed using empirical models for ground and spectral parameters based on earthquake records obtained from different datasets. This implies that the selected earthquakes may not necessarily represent pulse-like motions. Therefore, future studies are required to derive predictive models that are more consistent with the ensemble of pulse-like ground motions.

An assumption made in this study (and other related studies [28,30]) was that the spectral predominant periods T_g are insensitive to damping level, which may not to be appropriate for heavily damped response spectra. However, response spectra for high damping ratios do not exhibit the distinct peaks that appear in slightly damped spectra. Therefore, using predominant periods of slightly damped spectra for constructing heavily damped response spectra is considered acceptable for practical purposes. Another area requiring further attention relates to uncertainties in estimating the pulse period and/or other spectral control periods. This could be addressed by defining constant maximum spectral regions within the spectral range, limited for example by T_g-σ and T_g+σ (σ being the standard deviation of T_g). The values corresponding to the smoothed spectral amplification factors could then be evaluated within these regions.

Though the above mentioned limitations indicate that the suggested design response spectrum should not be directly applied in design practice, it has been shown that the concept of constructing such a design spectrum provides a better alternative to the conventional bi-normalised response spectra derived by normalising the spectral ordinates with respect to a single peak ground motion. Nevertheless, the procedure for DDBD of flexible-base structures proposed in this study is not restricted to the suggested design spectra, and, in essence, any type of design response spectrum can be easily employed to perform the design process.

6. CONCLUSIONS

A practical displacement-based design framework was presented, for the first time, for seismic design of flexible-base structures subjected to near-fault pulse-like ground motions. Within this framework, an actual soil-structure interaction system is treated as an equivalent fixed-base SDOF (EFSDOF) oscillator having an equivalent natural period, a system damping ratio, and an effective ductility ratio which can be readily determined using proposed formulations. The effects of near-fault pulse motions on structural response are accounted for by newly developed compatible response spectra that are directly correlated with the pulse period. Utilising the EFSDOF oscillator and the design response spectra, two step-by-step procedures were proposed on the basis of the suggested inelastic spectra and equivalent linearisation methods. The results of non-linear dynamic analysis performed on two example SSI systems under a set of sixteen spectrum-compatible pulse-like ground motions demonstrated that using heavily damped elastic displacement spectra based on conventional equivalent linearisation may lead to inappropriate design solutions in this case. However, it was shown that the proposed direct-displacement based design procedure based on inelastic design spectra in general provides more accurate results for the SSI systems under pulse-like ground motions. The results also indicate that the SSI effect is insignificant for structures with high ductility demand, where fixed-base and SSI-based DDBD design methods lead to almost identical design solutions.

APPENDIX A

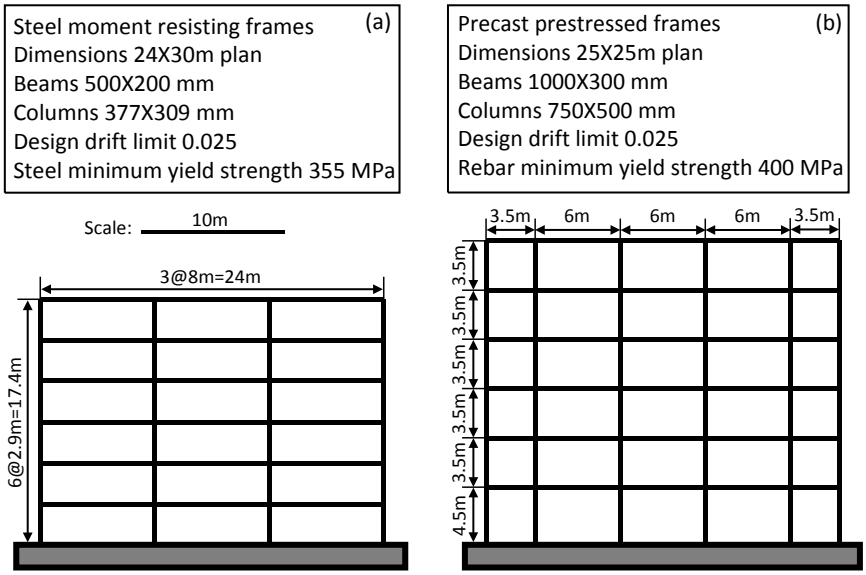

Figure A1. Frame buildings for the design SDOF example structures: (a) steel moment resisting frame building [63] and (b) hybrid precast prestressed frame building [55].

Table A1. Results of the DDBD procedure using inelastic spectra for Ex.1

	Iteration number									
Parameter	1	2	3	4	5	6	7	8	9	10
λ_0^2	1.000	1.683	1.240	1.369	1.303	1.334	1.319	1.326	1.322	1.324
$u_{ssi,m}$ (m)	0.256	0.381	0.300	0.323	0.311	0.317	0.314	0.315	0.315	0.315
ξ_{ssi}	0.050	0.242	0.120	0.159	0.139	0.148	0.144	0.146	0.145	0.146
T_{ssi}	0.682	1.343	0.969	1.104	1.035	1.067	1.051	1.059	1.055	1.057
a_0	1.468	0.968	1.151	1.062	1.105	1.084	1.094	1.089	1.091	1.090
λ_1^2	1.683	1.240	1.369	1.303	1.334	1.319	1.326	1.322	1.324	1.324
V_d (kN)										22179

Table A2. Results of the DDBD procedure using equivalent linearisation for Ex.1

	Iteration number								
Parameter	1	2	3	4	5	6	7	8	9
λ_0^2	1.000	1.526	1.277	1.371	1.330	1.347	1.340	1.343	1.341
$u_{ssi,m}$ (m)	0.256	0.352	0.306	0.324	0.316	0.319	0.318	0.318	0.318
$\xi_{ssi,eq}$	0.137	0.220	0.176	0.192	0.185	0.188	0.187	0.187	0.187
$T_{ssi,eq}$	0.899	1.355	1.123	1.209	1.171	1.187	1.180	1.183	1.182
a_0	1.318	1.026	1.155	1.102	1.125	1.115	1.119	1.118	1.118
λ_1^2	1.526	1.277	1.371	1.330	1.347	1.340	1.343	1.341	1.341
V_d (kN)									23335

Table A3. Results of the DDBD procedure using inelastic spectra for Ex.2

	Iteration number				
Parameter	1	2	3	4	5
λ_0^2	1.000	1.389	1.478	1.465	1.467
$u_{ssi,m}$ (m)	0.303	0.320	0.324	0.323	0.323
ξ_{ssi}	0.050	0.155	0.178	0.175	0.176
T_{ssi}	0.869	0.915	0.951	0.946	0.946
a_0	1.359	1.520	1.509	1.511	1.511
λ_1^2	1.389	1.478	1.465	1.467	1.467
V_d (kN)					5501

Table A4. Results of the DDBD procedure using equivalent linearisation for Ex.2

	Iteration number						
Parameter	1	2	3	4	5	6	7
λ_0^2	1.000	2.646	2.111	2.244	2.208	2.218	2.215
$u_{ssi,m}$ (m)	0.303	0.375	0.351	0.357	0.356	0.356	0.356
$\xi_{ssi,eq}$	0.258	0.262	0.255	0.256	0.256	0.256	0.256
$T_{ssi,eq}$	1.284	1.520	1.430	1.452	1.446	1.448	1.447
a_0	2.434	2.285	2.351	2.335	2.340	2.338	2.339
λ_1^2	2.646	2.111	2.244	2.208	2.218	2.215	2.215
V_d (kN)							13180

APPENDIX B

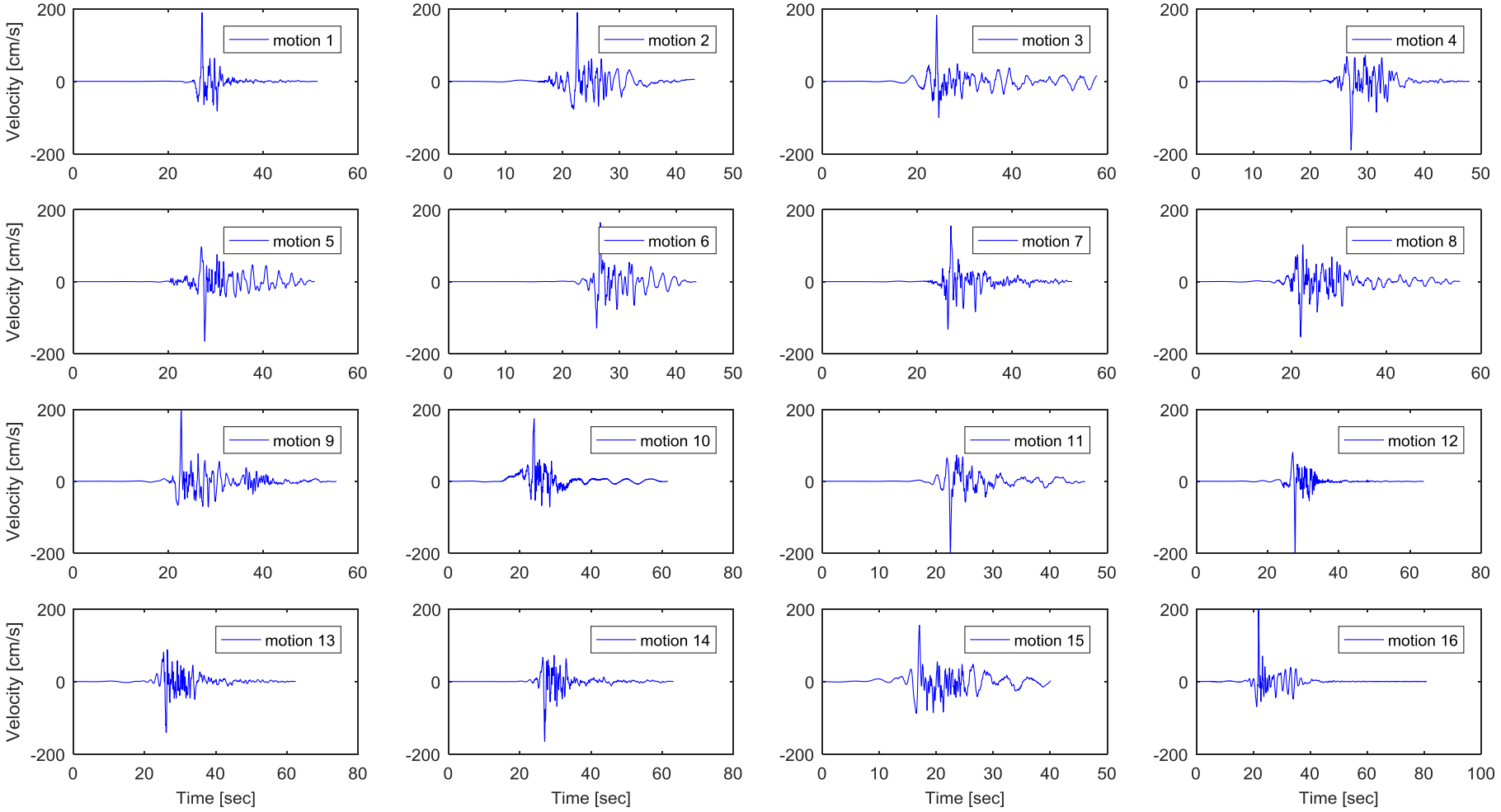

Figure B1. Velocity time series of the design earthquake motions showing the pulse characteristics.

REFERENCES

[1] P.G. Somerville, N.F. Smith, R.W. Graves, N.A. Abrahamson, Modification of empirical strong ground motion attenuation relations to include the amplitude and duration effects of rupture directivity, Seismol. Res. Lett. 68 (1997) 199–222.

[2] A. Ghobarah, Response of structures to near-fault ground motion, in: 13th World Conf. Earthq. Eng., Vancouver, 2004: pp. 1–6.

[3] S.F. Ghahari, H. Jahankhah, M.A. Ghannad, Study on elastic response of structures to near-fault ground motions through record decomposition, Soil Dyn. Earthq. Eng. 30 (2010) 536–546.

[4] B. Alavi, H. Krawinkler, Behavior of moment-resisting frame structures subjected to near-fault ground motions, Earthq. Eng. Struct. Dyn. 33 (2004) 687–706.

[5] S. Akkar, U. Yazgan, P. Gülkan, Drift estimates in frame buildings subjected to near-fault ground motions, J. Struct. Eng. 131 (2005) 1014–1024.

[6] E. Kalkan, S.K. Kunnath, Effects of fling step and forward directivity on seismic response of buildings, Earthq. Spectra. 22 (2006) 367–390.

[7] J.W. Baker, Quantitative classification of near-fault ground motions using wavelet analysis, Bull. Seismol. Soc. Am. 97 (2007) 1486–1501.

[8] C. Champion, A. Liel, The effect of near-fault directivity on building seismic collapse risk, Earthq. Eng. Struct. Dyn. 41 (2012) 1391–1409.

[9] J. Avilés, L.E. Pérez-Rocha, Soil-structure interaction in yielding systems, Earthq. Eng. Struct. Dyn. 32 (2003) 1749–1771.

[10] M.A. Ghannad, H. Jahankhah, Site-dependent strength reduction factors for soil-structure systems, Soil Dyn. Earthq. Eng. 27 (2007) 99–110.

[11] P. Raychowdhury, Seismic response of low-rise steel moment-resisting frame (SMRF) buildings incorporating nonlinear soil-structure interaction (SSI), Eng. Struct. 33 (2011) 958–967.

[12] B. Ganjavi, H. Hao, Effect of structural characteristics distribution on strength demand and ductility reduction factor of MDOF systems considering soil-structure interaction, Earthq. Eng. Eng. Vib. 11 (2012) 205–220.

[13] S. Jarernprasert, E. Bazan-Zurita, J. Bielak, Seismic soil-structure interaction response of inelastic structures, Soil Dyn. Earthq. Eng. 47 (2013) 132–143.

[14] K. Galal, M. Naimi, Effect of soil conditions on the response of reinforced concrete tall structures to near-fault earthquakes, Struct. Des. Tall Spec. Build. 17 (2008) 541–562.

[15] M.A. Ghannad, A. Amirib, S.F. Ghahari, Effects of soil-structure interaction on response of structures subjected to near-fault earthquake records, in: AIP Conf. Proc., 2008: p. 642.

[16] F. Khoshnoudian, E. Ahmadi, Effects of pulse period of near-field ground motions on the seismic demands of soil-MDOF structure systems using mathematical pulse models, Earthq. Eng. Struct. Dyn. 42 (2013) 1565–1582.

[17] F. Khoshnoudian, E. Ahmadi, Effects of inertial soil-structure interaction on inelastic displacement ratios of SDOF oscillators subjected to pulse-like ground motions, Bull. Earthq. Eng. 13 (2014) 1809–1833.

[18] E. Ahmadi, F. Khoshnoudian, Near-fault effects on strength reduction factors of soil-MDOF structure systems, Soils Found. 55 (2015) 841–856.

[19] S.K. Shahi, J.W. Baker, An empirically calibrated framework for including the effects of near-fault directivity in probabilistic seismic hazard analysis, Bull. Seismol. Soc. Am. 101 (2011) 742–755.

[20] E. Chioccarelli, I. Iervolino, Near-source seismic hazard and design scenarios, Earthq. Eng. Struct. Dyn. 42 (2013) 603–622.

[21] R. Paolucci, R. Figini, L. Petrini, Introducing dynamic nonlinear soil-foundation-structure interaction effects in displacement-based seismic design, Earthq. Spectra. 29 (2013) 475–496.

[22] L. Deng, B.L. Kutter, S.K. Kunnath, Seismic design of rocking shallow foundations: Displacement-based methodology, J. Bridg. Eng. 19 (2014) 4014043.

[23] M. Mekki, S.M. Elachachi, D. Breysse, D. Nedjar, M. Zoutat, Soil-structure interaction effects on RC structures within a performance-based earthquake engineering framework, Eur. J. Environ. Civ. Eng. 18 (2014) 945–962.

[24] M. Moghaddasi, G.A. MacRae, J.G. Chase, M. Cubrinovski, S. Pampanin, Seismic design of yielding structures on flexible foundations, Earthq. Eng. Struct. Dyn. (2015).

[25] Y. Lu, I. Hajirasouliha, A.M. Marshall, Performance-based seismic design of flexible-base multi-storey buildings considering soil-structure interaction, Eng. Struct. 108 (2016) 90–103.

[26] FEMA P-1050, NEHRP recommended seismic provisions for new buildings and other structures, Applied Technology Council, Washington DC, 2015.

[27] ASCE/SEI 7-16, Minimum design loads and associated criteria for buildings and other structures, American Society of Civil Engineers, Reston, Virginia, 2016.

[28] C.A. Maniatakis, C.C. Spyrakos, A new methodology to determine elastic displacement spectra in the near-fault region, Soil Dyn. Earthq. Eng. 35 (2012) 41–58.
[29] G.P. Mavroeidis, G. Dong, A.S. Papageorgiou, Near-fault ground motions, and the response of elastic and inelastic single-degree-of-freedom (SDOF) systems, Earthq. Eng. Struct. Dyn. 33 (2004) 1023–1049.
[30] L. Xu, L. Xie, Bi-normalized response spectral characteristics of the 1999 Chi-Chi earthquake, Earthq. Eng. Eng. Vib. 3 (2004) 147–155.
[31] L. Xu, L. Xie, Near-fault ground motion bi-normalized pseudo-velocity spectra and its applications, Acta Seismol. Sin. 20 (2007) 544–552.
[32] A. Ziotopoulou, G. Gazetas, Are current design spectra sufficient for soil-structure systems on soft soils?, in: Adv. Performance-Based Earthq. Eng., Springer, 2010: pp. 79–87.
[33] A.K. Chopra, Dynamics of Structures, Pearson Education, 2012.
[34] P.K. Malhotra, Smooth spectra of horizontal and vertical ground motions, Bull. Seismol. Soc. Am. 96 (2006) 506–518.
[35] L. Xu, G. Zhao, Q. Liu, Y. Xie, L. Xie, Consecutive combined response spectrum, Earthq. Eng. Eng. Vib. 13 (2014) 623–636.
[36] N.M. Newmark, W.J. Hall, Earthquake spectra and design, Earthquake Engineering Research Institute, 1982.
[37] I.J. Tromans, J.J. Bommer, The attenuation of strong-motion peaks in Europe, in: Proc. 12th Eur. Conf. Earthq. Eng., 2002: p. 394.
[38] E.M. Rathje, N.A. Abrahamson, J.D. Bray, Simplified frequency content estimates of earthquake ground motions, J. Geotech. Geoenvironmental Eng. 124 (1998) 150–159.
[39] J.D. Bray, A. Rodriguez-Marek, Characterization of forward-directivity ground motions in the near-fault region, Soil Dyn. Earthq. Eng. 24 (2004) 815–828.
[40] T.C. Hanks, H. Kanamori, A moment magnitude scale, J. Geophys. Res. 84 (1979) 2348–2349.
[41] N.N. Ambraseys, K.A. u Simpson, J.J. Bommer, Prediction of horizontal response spectra in Europe, Earthq. Eng. Struct. Dyn. 25 (1996) 371–400.
[42] E.M. Scordilis, Empirical global relations converting MS and mb to moment magnitude, J. Seismol. 10 (2006) 225–236.
[43] L. Xu, A. Rodriguez-Marek, L. Xie, Design spectra including effect of rupture directivity in near-fault region, Earthq. Eng. Eng. Vib. 5 (2006) 159–170.
[44] D.T. Hubbard, G.P. Mavroeidis, Damping coefficients for near-fault ground motion response spectra, Soil Dyn. Earthq. Eng. 31 (2011) 401–417.
[45] G.D. Hatzigeorgiou, Damping modification factors for SDOF systems subjected to near-fault, far-fault and artificial earthquakes, Earthq. Eng. Struct. Dyn. 39 (2010) 1239–1258.
[46] H. Qu, J. Zhang, J.X. Zhao, Strength reduction factors for seismic analyses of buildings exposed to near-fault ground motions, Earthq. Eng. Eng. Vib. 10 (2011) 195–209.
[47] M. Ordaz, L.E. Pérez-Rocha, Estimation of strength-reduction factors for elastoplastic systems: a new approach, Earthq. Eng. Struct. Dyn. 27 (1998) 889–902.
[48] J.L. Gillie, A. Rodriguez-Marek, C. McDaniel, Strength reduction factors for near-fault forward-directivity ground motions, Eng. Struct. 32 (2010) 273–285.
[49] I. Iervolino, E. Chioccarelli, G. Baltzopoulos, Inelastic displacement ratio of near-source pulse-like ground motions, Earthq. Eng. Struct. Dyn. 41 (2012) 2351–2357.
[50] J. Ruiz-Garcia, Inelastic displacement ratios for seismic assessment of structures subjected to forward-directivity near-fault ground motions, J. Earthq. Eng. 15 (2011) 449–468.
[51] P. Fajfar, Capacity spectrum method based on inelastic demand spectra, Earthq. Eng. Struct. Dyn. 28 (1999) 979–993.
[52] ASCE/SEI 41-17, Seismic Evaluation and Retrofit of Existing Buildings, American Society of Civil Engineers, Reston, Virginia, 2017.
[53] FEMA 440, Improvement of Nonlinear Static Seismic Analysis Procedures, Applied Technology Council, Washington DC, 2005.
[54] F. Khosravikia, M. Mahsuli, M.A. Ghannad, Comparative Assessment of Soil-Structure Interaction Regulations of ASCE 7-16 and ASCE 7-10, in: ASCE Struct. Congr., 2018.
[55] M.J.N. Priestley, G.M. Calvi, M.J. Kowalsky, Displacement-based Seismic Design of Structures, IUSS Press, 2007.
[56] A. Maravas, G. Mylonakis, D.L. Karabalis, Simplified discrete systems for dynamic analysis of structures on footings and piles, Soil Dyn. Earthq. Eng. 61 (2014) 29–39.
[57] A.S. Veletsos, B. Verbič, Vibration of viscoelastic foundations, Earthq. Eng. Struct. Dyn. 2 (1973) 87–102.
[58] S.L. Kramer, Geotechnical earthquake engineering, Pearson Education India, 1996.
[59] I. Ishibashi, X. Zhang, Unified dynamic shear moduli and damping patios of sand and clay, Soils Found. 33 (1993) 182–191.

[60] P. Gulkan, M.A. Sozen, Inelastic Responses of Reinforced Concrete Structures to Earthquake Motions, J. Am. Concr. Inst. 71 (1974).
[61] A.K. Chopra, R.K. Goel, Capacity-demand-diagram methods for estimating seismic deformation of inelastic structures: SDF systems, Report No. PEER-1999/02, (1999).
[62] A.K. Chopra, R.K. Goel, Direct displacement-based design: use of inelastic vs. elastic design spectra, Earthq. Spectra. 17 (2001) 47–64.
[63] P. Bisch, E. Carvalho, H. Degee, P. Fajfar, M. Fardis, P. Franchin, M. Kreslin, A. Pecker, P. Pinto, A. Plumier, Eurocode 8: seismic design of buildings worked examples, Luxemb. Publ. Off. Eur. Union. (2012).
[64] L. Al Atik, N. Abrahamson, An improved method for nonstationary spectral matching, Earthq. Spectra. 26 (2010) 601–617.
[65] I. Anastasopoulos, T. Kontoroupi, Simplified approximate method for analysis of rocking systems accounting for soil inelasticity and foundation uplifting, Soil Dyn. Earthq. Eng. 56 (2014) 28–43.
[66] Y. Lu, A.M. Marshall, I. Hajirasouliha, A simplified Nonlinear Sway-Rocking model for evaluation of seismic response of structures on shallow foundations, Soil Dyn. Earthq. Eng. 81 (2016) 14–26.
[67] F. Khoshnoudian, E. Ahmadf, S. Sohrabi, M. Kiani, Higher-mode effects for soil-structure systems under different components of near-fault ground motions, Earthq. Struct. 7 (2014) 83–99.
[68] F. Khoshnoudian, R. Attarnejad, F. Paytam, E. Ahmadi, Effects of forward directivity on the response of soil–structure systems, Proc. Inst. Civ. Eng. Struct. Build. 168 (2015).